Available online at www.sciencedirect.com
ScienceDirect
Thin Solid Films 516 (2007) 58–66
www.elsevier.com/locate/tsf

Study of the non-covalent interactions in Langmuir–Blodgett films: An interplay between π−π and dipole–dipole interactions

Zhexiong Tang [d], Malkiat S. Johal [b,*], Paul Scudder [a], Niña Caculitan [a], Rudolph J. Magyar [c], Sergei Tretiak [c], Hsing-Lin Wang [d,*]

[a] Division of Natural Sciences, New College of Florida, Sarasota, FL 34243-2197, USA
[b] Department of Chemistry, Pomona College, 645 North College Avenue, Claremont, CA 91711, USA
[c] Theoretical Division and Center for Nonlinear Studies, Los Alamos National Laboratory, Los Alamos, NM 87545, USA
[d] Chemistry Division, Los Alamos National Laboratory, Los Alamos, NM, 87545, USA

Received 20 October 2006; received in revised form 7 April 2007; accepted 24 April 2007
Available online 3 May 2007

Abstract

This work describes Langmuir–Blodgett (L–B) monolayer and multilayer assemblies constructed from a series of NLO-active azo-benzene derivatives possessing terminal moieties of variable dipole moment. The terminal groups are electron acceptors (acetyl, nitro, and cyano) and are connected to a common amphiphilic azo-benzene segment. Our experimental and theoretical results show that the interplay between two dominant non-covalent interactions within the assemblies, namely dipolar and π−π stacking interactions, dictate the packing density, structural order, as well as the electronic properties of the final films. L–B films of the acetyl derivative, which has the weakest total dipole across the azo-benzene chromophore, exhibits the highest packing density and the largest blue shift in the UV–visible absorption spectrum. This is rationalized by relatively strong π−π interactions between the azo-benzene chromophores overwhelming weak intermolecular dipole–dipole interactions. More importantly, the small internal dipole in the acetyl functional groups encourages packing in a configuration that lowers the overall energy and increases the packing density. In the case of the cyano and nitro derivatives, both L–B films show decrease in packing density and a weaker electronic coupling due to unfavorable overall dipole interaction that offsets the π−π interaction. We show that such unfavorable interactions lead to the formation of a staggered and loosely packed configuration. Our work demonstrates that a subtle difference in molecular structure can have a dramatic impact on aggregation, and consequently on the electronic and optical properties of nano-assemblies. This work demonstrates a way of controlling the formation of nanoscale structures at the molecular level through the control of noncovalent interactions.

Keywords: Langmuir–Blodgett; Azobenzene; Noncovalent interaction; Aggregate; Packing; Isotherm; Dipole

1. Introduction

Understanding the intrinsic structure-property relationships in highly ordered molecular assemblies has been underscored by developments in organic electro-optic materials [1–4]. Despite some shortcomings, self-assembly methods continue to hold a lot of promise in achieving desired architectures in organic assemblies. The desire to guide molecular assembly into hierarchical macro-structures has been propelled by the realization that specific molecular geometries favor specialized functions, such as the nonlinear optical (NLO) effects observed in asymmetrically ordered multilayers [5,6]. For example, NLO-active organic materials containing asymmetric chromophores have characteristics (e.g. low dielectric constants, ultrafast response times, and large hyperpolarizabilities) that make them an attractive alternative to their inorganic counterparts [7–9]. However, achieving the inherent intralayer asymmetric alignment in self-assemblies has proven challenging largely because interactions within such assemblies are poorly understood.

Perhaps the most extensively used method of directing molecular orientation in multilayers is the Langmuir–Blodgett

* Corresponding authors.
E-mail addresses: Malkiat.Johal@pomona.edu (M.S. Johal), hwang@lanl.gov (H.-L. Wang).

0040-6090/$ - see front matter © 2007 Elsevier B.V. All rights reserved.
doi:10.1016/j.tsf.2007.04.149

(L–B) technique, in which compressed amphiphilic molecules at the air–water interface are reversibly transferred to a solid support [10]. Despite considerable experimental and theoretical efforts, fabricating uniform, defect-free films with predictable structural properties continues to pose a significant challenge [11,12]. Although the L–B technique has produced a plethora of systems containing chromophoric units derived from stilbenes, merocyanines, hemicyanines, azobenzenes, the ultimate goal of precise control over the chromophore orientation is yet to be demonstrated [13,14].

One major hurdle in achieving long-range order is chromophore randomization at the mesoscale. Our previous work has shown the presence of significant inter-layer mixing between L–B layers resulting in structural defects and chromophore tilting that becomes amplified as a function of bilayer number [15]. Moreover, fatty acid spacers, such as stearic acid, may be used to maintain noncentrosymmetry throughout the bulk film. However, these spacers have been observed to augment disorder in some L–B films since stearic acid may form two-dimensional crystalline structures resulting in a heterogeneous monolayer filled with defects [16]. More importantly, staggered molecular structures may form due to repulsive interaction between strong dipoles. One way to combat these effects and to increase order is to promote the formation of ordered aggregates. For example, Li et al. achieved noncentrosymmetric aggregates on L–B films using a stilbazolium dye dimer whose monomeric units are connected with a methylene bridge [16]. The observed NLO response of the resulting L–B films was found to be greater than that of the L–B film consisting of the monomer formed under similar experimental conditions. Despite enormous efforts in controlling the experimental parameters, such as temperature and surface pressure, the intrinsic intralayer disorder caused by unfavorable dipole–dipole interactions between NLO amphiphiles and interlayer interactions, inhibit the formation of 3D structures with long range order. It appears that the interplay between enthalpy and entropy, and the nature of non-covalent forces that unite molecular building blocks to form self-assembled aggregates need to be understood. To address some of these issues, we have synthesized a series of NLO-active molecular building blocks that are amphiphilic, of approximately the same size, and have terminal dipole moieties of variable electron-withdrawing strength. Understanding how non-covalent interactions (e.g. Coulomb forces and π–π interactions) influence the structure and order of the functional nanoassemblies forms the central theme of this paper. Understanding these interactions could allow one to predict equilibrium structures and properties of functional nanoassemblies based on the specific amphiphilic structure.

Intermolecular aggregation within 2D assemblies can lead to two arrangements for adjacent chromophores aligned parallel to each other. A “head-to-head” and “tail-to-tail” arrangements of the dipoles lead to so-called H-aggregates. Their optical absorption spectra display prominent spectral blue shifts in the absorbance compared to the monomeric units. On the other hand, J-aggregates are formed when dipoles are arranged in a “head-to-tail” configuration, leading to red shifts in the linear absorption [17]. This work describes the L–B assembly on a hydrophobically rendered quartz substrate and characterization of the class of NLO-active amphiphiles X-azo-$(CH_2)_{10}$–SO_3^-, where X=–$COCH_3$, –NO_2, or –CN (Fig. 1). These molecules contain the essential functional groups (electron donor and acceptor groups bridged by an azo-benzene group) required for a large second order hyperpolarizability. We have recently reported the large second harmonic response from multilayer systems comprised of these amphiphiles [18]. Absorption spectroscopy studies revealed H-aggregate [19] formation of X-azo-$(CH_2)_{10}$–SO_3^- in films assembled using electrostatic self-assembly (ESA) with oppositely charged polyelectrolytes. It is believed that the head-to-head packing of the chromophore was promoted by the presence of inter-alkyl chain interactions and the anchoring of the SO_3^- head groups of the surfactants into the underlying hydrophilic polycationic layer [18].

The work presented here further explores dipolar interactions on aggregate formation in L–B assemblies of X-azo-$(CH_2)_{10}$–SO_3^-. Thus, this study provides valuable insight into the design of molecular building blocks that could lead to structures with desirable nonlinear optical and electronic properties. Curiously, in the multilayered films formed by ESA, the blue shift reflecting the degree of H-aggregation increased with strength of the molecular dipole moment, μ as follows –$COCH_3$<–NO_2<–CN. Given the same “head-to-head” (“tail-to-tail”) molecular stacking, the strength of dipolar interactions between chromophores will directly affect the excited state shifts of the aggregate. However, we show that an opposite trend emerges in the absorption spectra of the L–B films of X-azo-$(CH_2)_{10}$–SO_3^- adsorbed onto a hydrophobic substrate compared to their spectra in chloroform solution. Furthermore, pressure–area (Π–A) isotherms and hysteresis studies were used to explore the packing density and aggregation properties of the L–B films. We observe that the packing density of monolayer structure at the air–water interface is the highest for acetyl-azobenzene (X=–$COCH_3$), followed by nitro-azobenzene (X=–NO_2) and cyano-azobenzene (X=–CN) amphiphiles. This result is congenial to the

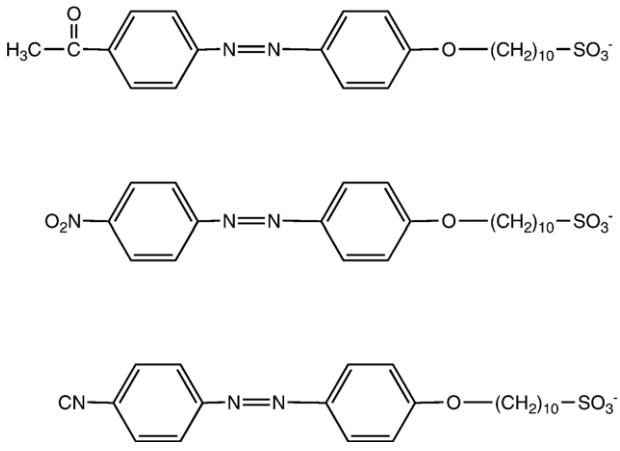

Fig. 1. Structure of the three NLO-active amphiphiles used in this study. The various terminal electron withdrawing groups (X) are shown (–$COCH_3$, –NO_2, and –CN). The dipole moment of the X group follows the order –$COCH_3$<–NO_2<–CN.

increasing blue shift with decreasing dipole moment of chromophores. This suggests a trend in increasing H-aggregation with decreasing dipole–dipole interaction between chromophores. The strong dipoles within the compact 2D monolayer tend to repel each other and energy minimization is achieved through a staggered arrangement in which repulsive and attractive forces reach an equilibrium balance. Acetyl-azobenzene with a relatively weak molecular dipole and a strong internal dipole on the acetyl group has a very strong tendency to form H-aggregates. This tendency is reflected in the pressure isotherm in which the surface area/molecule is determined to be very small (34 $Å^2$). Further insight into experimental studies has been achieved using density functional theory (DFT) and time-dependent (TD)-DFT computations. We show that the internal dipoles within the acetyl groups are aligned in antiparallel directions, which lowers the overall energy and increases the packing density. The changes in electronic coupling resulting from different packing densities in the L–B films are clearly seen in the UV–visible absorbance spectrum. The acetyl-azobenzene has the greatest blue shift compared to the cyano- and the nitro-azo-benzene derivatives. The similarity in structure also leads us to believe that π−π interaction between these chromophores is essentially identical. Therefore, we conclude that the relative position of the chromophore tilt depends on a delicate balance between dipole–dipole and π−π interactions. This balance ultimately dominates the packing density, order and electronic properties of the final L–B structure.

2. Experimental details

2.1. Synthesis of X-azo-$(CH_2)_{10}$–SO_3^-

The synthesis of X-azo-$(CH_2)_{10}$–SO_3^- is described in greater detail elsewhere [18]. The first step in the synthesis involves diazonium ion formation from a para-substituted amino-benzene substituted by the various electron withdrawing groups, X = –NO_2, –CN, and –$COCH_3$. Subsequently, coupling with phenol produces the azodye [20,21]. This azodye undergoes two nucleophilic substitution reactions to attach the alkyl chain [22] and obtain the sulfonate head group at the distal end of the alkyl chain [23].

2.2. Film formation

Multilayered films were fabricated on 1 in. diameter quartz substrate by the Langmuir–Blodgett method. The substrates were cleaned by immersion in a 7:3 mixture of concentrated sulfuric acid and 30% H_2O_2 at 80 °C for 1 h (Piranha etch treatment). Prior to use, substrates were treated with octadecyltrichlorosilane (OTS, 1% in hexadecane solution) at 40 °C for 45 min and then washed thoroughly in $CHCl_3$ in order to generate a hydrophobic surface. The azo-benzene-derived surfactants ($\sim 10^{-3}$ mmol) were dissolved in 10 ml chloroform to give a 0.1 mM solution. Approximately 2 ml of these as-prepared chloroform solutions was spread on the water surface. The measurements of the surface pressure–area (∏-A) isotherms were carried out using a KSV 2000 standard computer controlled L–B trough (KSV Instrument, Helsinki, Finland) with a Wilhelmy-type balance, a Teflon trough, and symmetrical hydrophilic Delrin barriers. The trough was set in a dust and draft free enclosure, and temperature controlled to within ± 0.5 °C. Ultrapure water (resistivity > 18 MΩ cm) from a Barnstead e-pure system was used as the subphase. Monolayers were spread from chloroform solutions on the pure water subphase at 21 °C. After waiting 15 min to allow solvent evaporation, isotherms were obtained by reducing the surface area available to the material at a rate of 10 cm^2/s. During the L–B depositions, the transfer surface pressure was fixed at 25 mN m^{-1}. For multilayer buildup, the Langmuir films of the amphiphiles were formed by compression at a surface pressure of 30 mN m^{-1} and the monolayers were then transferred onto hydrophobically treated quartz substrates.

2.3. Characterization

The layer deposition process was monitored by UV–visible absorption spectroscopy. UV–visible spectra (Varian Cary 300 spectrophotometer) of the multilayered films built on glass substrates were taken between 315 and 800 nm for every layer. Spectra of the bulk solutions in chloroform were also taken for comparison.

2.4. Computational methodology

Quantum-chemical computations have become a powerful tool for insightful theoretical investigations in virtually every molecular class. In particular, adiabatic TD-DFT in the Kohn–Sham form is currently the method of choice for calculating the excited state structure of large molecular systems [24–26].

Density functional theory with the BHandHLYP functional and the 6-31G basis set was used in all simulations. The 6-31G basis set is known to be an efficient blend of accuracy and a manageable size for large conjugated systems, and the BHandHLYP functional, which incorporates 50% exact exchange, eliminates most charge transfer problems in the excited states that plague other hybrid, semi-local, and pure functionals. We start our calculations with optimization of ground state geometries. TD-DFT formalism implemented in the Gaussian 98 program package [27] was then used to calculate the excited-state electronic structure. To model the azo-benzene derivatives in solution, the electronic structure of the monomers was calculated with a solvent model (the polarizable continuum model (PCM) based on the integral equation formalism) [28,29] parameterized for chloroform, as implemented in Gaussian 98 [27]. Solvent-induced trends remained the same when other versions of PCM were used. We also calculated excited states of dimers of the azo-benzene derivatives to obtain insights into the electronic structure of films since the bulk film results can be approximately related to the dimer results via simple Hückel theory. The dimers were fixed in their BHandHLYP optimized geometries and oriented co-facially a set distance apart. Physical packing is most likely in a herringbone configuration, but the primary physics of the situation should clearly be evidenced in this idealized packing.

3. Results and discussion

An inherently strong electron withdrawing group (e.g. –CN) creates a large dipole moment across the azo-benzene chromophore. The aggregation of azo-benzene chromophores in a close-packed 2D monolayer is thus dictated by favorable π−π stacking interactions and unfavorable dipolar interactions between nearest neighbors. If the dipole couplings among chromophores are sufficiently weak, π−π stacking interactions will dominate and lead to an H-aggregated assembly. If the dipole moment across the azo-benzene chromophore is sufficiently strong, π−π stacking interactions will not dominate and a staggered assembly will be formed. The interplay between these interactions can be discerned by studying the hysteresis in the *Π–A* isotherms of the three molecules at the air–water interface, and the UV–visible absorbance spectra of the corresponding L–B films.

3.1. Pressure–area isotherms

The *Π–A* isotherms of the amphiphiles are shown in Fig. 2. The *Π–A* isotherm of CN-azo-$(CH_2)_{10}$–SO_3^- exhibits a liquid expanded (LE) phase at a surface pressure of 0 mN/m< *Π*<9 mN/m. The onset of a second region is observed, characterized by a sharp increase in surface pressure as the monolayer is compressed further (9 mN/m< *Π*<43 mN/m). This increase in pressure is consistent with the formation of a liquid-condensed (LC) phase. Extrapolating the surface pressure at the LC phase to a zero pressure yields a limiting surface area per molecule of 40 $Å^2$/molecule. The *Π–A* isotherm of NO_2-azo-$(CH_2)_{10}$–SO_3^- displays a similar pattern to the isotherm of CN-azo-$(CH_2)_{10}$–SO_3^-. The monolayer at the air–water interface changes from a LE to a LC phase at *Π*=8 mN/m. The extrapolation of the LC portion of the isotherm to zero surface pressure yields a limiting surface area per molecule of 37 $Å^2$/molecule, which is smaller than the limiting surface area per molecule of CN-azo-$(CH_2)_{10}$–SO_3^-. These results suggest that both compounds lead to a monolayer formation at the air/water interface rather than to irreversible three-dimensional clustering of the molecules. Like those of CN-azo-$(CH_2)_{10}$–SO_3^- and NO_2-azo-$(CH_2)_{10}$–SO_3^-, the monolayer of CH_3CO-azo-$(CH_2)_{10}$–SO_3^- at the air–water interface changes from a LE to a LC phase at *Π*=3 mN/m. The extrapolation of the LC portion of the isotherm to zero surface pressure leads to a limiting surface area per molecule of 33 $Å^2$/molecule, which is the smallest among the three molecules. Based on these limiting areas it can be concluded that CH_3CO-azo-$(CH_2)_{10}$–SO_3^- bears the strongest amphiphilic character.

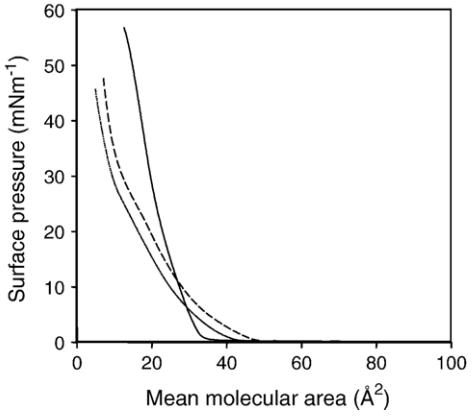

Fig. 2. *Π–A* isotherm of CN-azo-$(CH_2)_{10}$–SO_3^- (dotted line), NO_2-azo-$(CH_2)_{10}$–SO_3^- (solid line), and CH_3CO-azo-$(CH_2)_{10}$–SO_3^- (dashed line) monolayers spread at the air–water interface. Isotherms were obtained at 21 °C±0.5 °C.

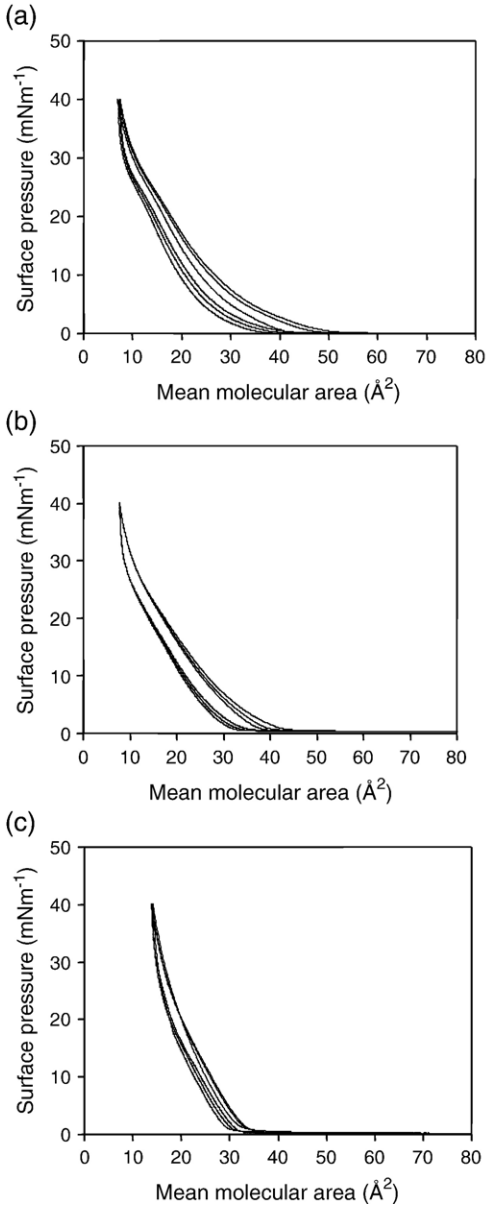

Fig. 3. Hysteresis data on (a) CN-azo-$(CH_2)_{10}$–SO_3^-; (b) and NO_2-azo-$(CH_2)_{10}$–SO_3^-; and (c) CH_3CO-azo-$(CH_2)_{10}$–SO_3^-. Isotherms were obtained at 21 °C± 0.5 °C.

Isotherm compression–decompression data was collected for all three species (Fig. 3). In all cases, hysteresis was observed. Isotherm hysteresis for CN-azo-$(CH_2)_{10}$–SO_3^- (Fig. 3a) shows a shift to a lower surface area region, even if the surface pressure is

kept below the collapse pressure. The slow decrease of the mean molecular area after each cycle indicates a gradual increase in the irreversible clustering at the air–water interface. Furthermore, successive compression and decompression of NO_2-azo-$(CH_2)_{10}$–SO_3^- (Fig. 3b) displays less hysteresis in the isotherm compared to CN-azo-$(CH_2)_{10}$–SO_3^-. The differences in the two isotherms demonstrate that the NO_2-azo-$(CH_2)_{10}$–SO_3^- film reversibly expands following compression and has a reduced tendency to cluster compared to the CN-azo-$(CH_2)_{10}$–SO_3^- film. Only a slight decrease in the mean molecular area is observed after three compression–decompression cycles, which indicates the stability of NO_2-azo-$(CH_2)_{10}$–SO_3^- monolayer. These results suggest that NO_2-azo-$(CH_2)_{10}$–SO_3^- has a stronger amphiphilic character than CN-azo-$(CH_2)_{10}$–SO_3^-. It can form a more close-packed monolayer at the air–water interface under the same surface pressure. In Fig. 3c, the isotherms for CH_3CO-azo-$(CH_2)_{10}$–SO_3^- are almost exactly the same for three compression and decompression cycles. Thus, the monolayer of CH_3CO-azo-$(CH_2)_{10}$–SO_3^- at the air–water interface is the most stable of three materials, displaying the least hysteresis in the isotherm and the least tendency to cluster [10].

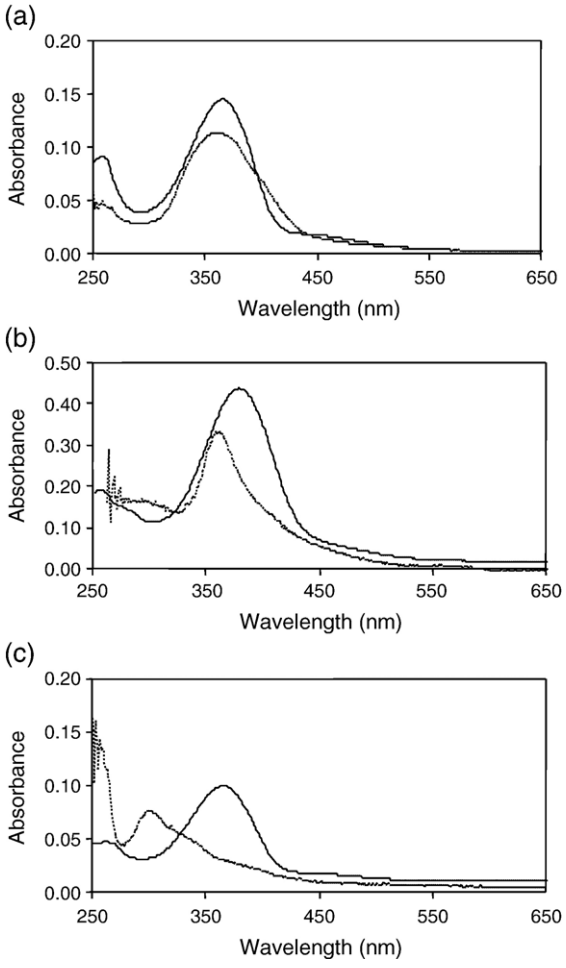

Fig. 4. UV–visible spectra of the L–B film (solid line) versus bulk solutions (dotted line) of (a) CN-azo-$(CH_2)_{10}$–SO_3^-; (b) and NO_2-azo-$(CH_2)_{10}$–SO_3^-; and (c) CH_3CO-azo-$(CH_2)_{10}$–SO_3^-.

Table 1
Resulting λ_{max} absorptions produced by the amphiphiles in aqueous and chloroform solutions and in L–B and ESA films

X	μ ($\times 10^{18}$ e.s.u.) [30]	L–B films		ESA films	
		λ_{max}/nm (chloroform)	λ_{max}/nm (L–B)	λ_{max}/nm (aqueous)	λ_{max}/nm (ESA)
CN	4.0	366	360	360	340
NO_2	3.1	379	351	370	360
$COCH_3$	2.7	366	302	360	353

The group dipole moments for each electron withdrawing functional group are also given.

3.2. Comparative study of UV–visible spectra of the amphiphiles in bulk solution and in L–B films

The absorption spectra of all three amphiphiles in both bulk solution and as L–B films (four deposition cycles) are shown in Fig. 4 and summarized in Table 1. For the CN-azo-$(CH_2)_{10}$–SO_3^- species, the absorbance spectrum in chloroform solution shows one major band at 365 nm, and a broad shoulder band at 450 nm (Fig. 4a). The Multilayer L–B films of CN-azo-$(CH_2)_{10}$–SO_3^- shows one major band at 356 nm, and no shoulder band at longer wavelengths. Compared to the solvent spectra, the multilayer L–B film absorption exhibits a very small blue shift. This shift is due to the presence of noncovalent interactions and chromophore coupling effects between the azobenzene chromophores in aggregated systems that are absent in dilute solutions. Additionally, the peak is much broader for the L–B film, which is due to the electronic coupling resulting from close contacts between molecular chains. The broadened band probably obscures the weak shoulder at 450 nm.

Similar to CN-azo-$(CH_2)_{10}$–SO_3^-, the bulk phase UV–visible absorption spectrum of NO_2-azo-$(CH_2)_{10}$–SO_3^- exhibits one major band at 379 nm and a weak absorption shoulder at 476 nm (Fig. 4b). The absorption spectrum of the corresponding multilayered L–B film shows significant blue shift with one major band at 351 nm. The increased blue shift suggests stronger H-aggregation character in the NO_2-azo-$(CH_2)_{10}$–SO_3^- L–B film compared to the CN-azo-$(CH_2)_{10}$–SO_3^- film. This is not surprising since the packing of NO_2-azo-$(CH_2)_{10}$–SO_3^- in each monolayer is expected to be denser than that of CN-azo-$(CH_2)_{10}$–SO_3^-.

The absorption spectrum of CH_3CO-azo-$(CH_2)_{10}$–SO_3^- in solution displays a major peak at 365 nm and a weak shoulder around 450 nm (Fig. 4c). The spectrum of the multilayered L–B film exhibits the largest blue shift (λ_{max}=302 nm) among all three molecules investigated. Compared to the other two molecules, the packing of CH_3CO-azo-$(CH_2)_{10}$–SO_3^- in each monolayer should be the densest since it has the smallest area per molecule at the air–water interface. The prominent blue shift observed for these species reflects the greatest degree of H-aggregation in the film.

The observed patterns of aggregation can be rationalized by considering the relative out-of-plane arrangements of the dipolar moieties (X). These structural relationships are schematically illustrated in Fig. 5. It is well understood that the degree of H-aggregation decreases with an increase in the out-of-plane shift and beyond a “magic” angle between the chromophore axis and

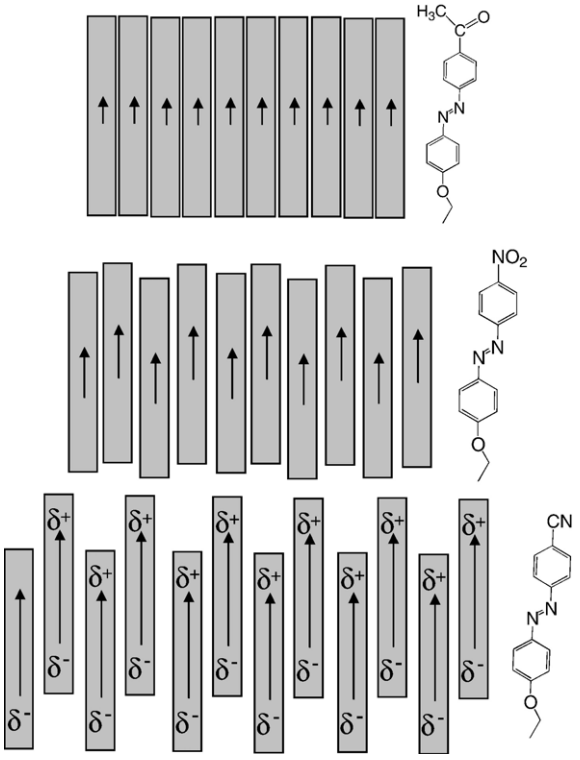

Fig. 5. Delicate balance between dipole–dipole interactions and π–π interactions lead to formation of monolayer structures with varying packing density and degree of H-aggregation.

a line connecting their centers, J-aggregation will occur. The amphiphile with the strongest dipole (X = –CN) assembles into a staggered and loosely packed structure at the air–water interface. In contrast, packing structure of the amphiphile possessing the weakest dipole (X = $-CH_3CO$) will be dominated by the π–π interactions between the azo-benzene chromophores. Such an interaction will give rise to densely packed H-aggregates. This model of packing is consistent with *Π–A* isotherm data and absorption spectrum of CH_3CO-azo-$(CH_2)_{10}$–SO_3^-. The NO_2-azo-$(CH_2)_{10}$–SO_3^- has an intermediate dipole strength, leading to the L–B film packing with slight shifts in the longitudinal direction. The blue shift in the absorption spectrum of these species is moderate implying an intermediate packing density.

3.3. Formation of multilayer L–B films on substrates

The transfer ratios for CN-azo-$(CH_2)_{10}$–SO_3^- and NO_2-azo-$(CH_2)_{10}$–SO_3^- L–B films are about 0.9 for the up cycles and nearly 0 for the down cycles. This minimum transfer ratio during the down cycles indicates weak hydrophobic interactions between the tail groups of CN and NO_2, therefore the film is likely to be X-type. X-type L–B films, which involve head-to-tail interactions, are more favorable for a centric chromophore alignment and have a net dipole moment for the bulk media. The UV–visible spectra of the L–B multilayer films for CN-azo-$(CH_2)_{10}$–SO_3^- and NO_2-azo-$(CH_2)_{10}$–SO_3^- are shown in Fig. 6a and b, respectively. The linear increase in absorbance demonstrates a linear increase in the amount of chromophores deposited onto the substrate as a function of deposition cycles.

Due to its strong amphiphilic character, the transfer ratio of the L–B films for CH_3CO-azo-$(CH_2)_{10}$–SO_3^- are both nearly 1 during the down and up cycles, indicating the formation of a Y-type film. This Y-type film is likely due to strong hydrophobic interactions between alkyl tail groups. The Langmuir films of CH_3CO-azo-$(CH_2)_{10}$–SO_3^- also exhibit reproducible deposition for each layer as reflected in the UV–visible spectra (Fig. 6c). The fact that X-type LB multilayer films (CN and NO_2) exhibit no shift between monolayer 1 and the following bilayer, suggests minimal interlayer chromophore interactions compared to that of strong coupling between chromophores within the same layer.

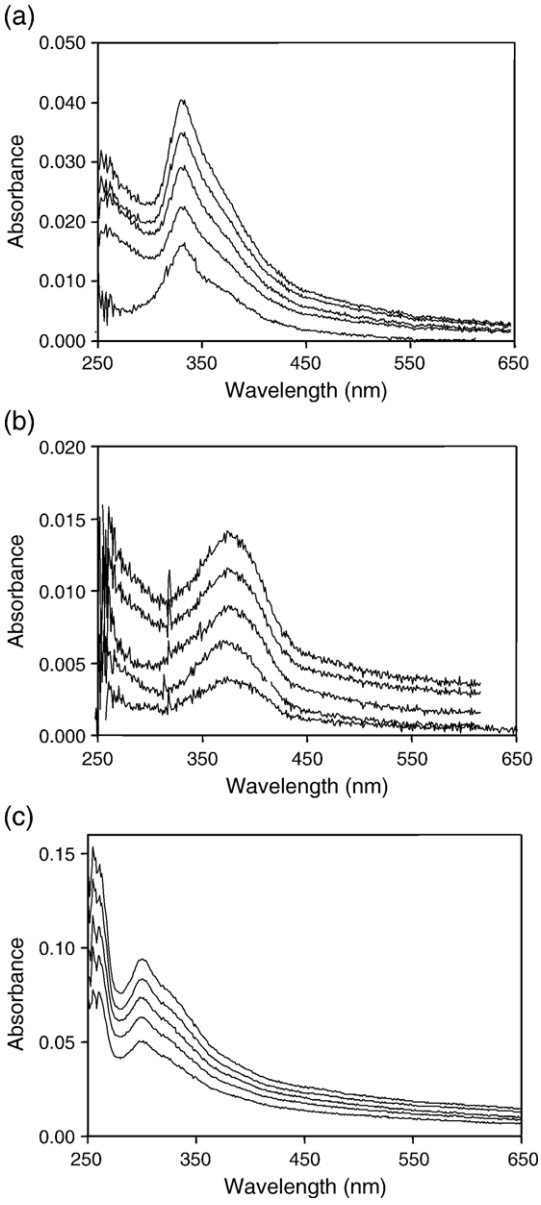

Fig. 6. UV–Vis of multilayer film formation for (a) CN-azo-$(CH_2)_{10}$–SO_3^-; (b) and NO_2-azo $(CH_2)_{10}$–SO_3^-; and (c) CH_3CO-azo-$(CH_2)_{10}$–SO_3^-.

3.4. Theoretical modeling of azo-benzene amphiphiles

To better understand how molecular packing affects the absorption spectra of the azo-benzene derivatives in solution and in the L–B films, we performed a series of quantum chemical calculations on all three azo-benzene derivatives. The purpose of these simulations is to gain an insight into the packing of the derivatives and the qualitative prediction of the shifting of the absorption peaks observed in the UV–visible spectra. In our calculations, methyl groups have replaced the long carbon chains as these chains should not drastically affect the excited-states of π−π* character. Our simulations show that the chemistry of film formation depends in a complex way on the competition between the total molecular dipole moments, the π–π interactions, and the internal dipole moments of the terminal ligands. Fig. 5 schematically shows possible packing models for the azo-benzene derivatives, whereas Fig. 7 displays related possible intermolecular orientations we used for calculations. Acetyl-azo-benzene with the CH_3CO ligand is expected to pack most tightly because the internal dipoles of the ligands can orient in an energetically favorable anti-parallel fashion. This is true for the idealized parallel packing and will likely also hold true for a less-idealized herringbone packing. For the cyanoazobenzene and for the nitroazobenzene, there is only one way for the chromophores to come together in this idealized scheme. For the latter, a slightly more complicated packing is possible in the herringbone packing. In which case, the interactions between the oxygens and the nitrogens of the nearest neighbors could lower the energy slightly. Therefore, this would have a limiting effect similar to what happens to CN-azo-$(CH_2)_{10}$–SO_3^- that could account for the intermediate packing.

Fig. 8A shows how the total energy changes for parallel packed dimers as they are positioned closer together following the Fig. 7 arrangement. For NO_2-azo-$(CH_2)_{10}$–SO_3^- and CN-azo-$(CH_2)_{10}$–SO_3, the total energy continuously increases as the intermolecular spacing is decreased, which reflects the penalty imposed by unfavorable dipolar orientation. For the anti-parallel configuration of the CH_3CO-azo-$(CH_2)_{10}$–SO_3, the energy initially decreases as the separation decreases. This implies that the internal dipoles of the acetyl groups, when oriented in opposite directions between pairs of molecules, energetically encourage dense packing. As expected, strong overlaps of the wavefunctions lead to intermolecular repulsion at distances closer than 4 Å. Another effect that affects packing is the tendency for different azo-benzene derivatives to form smoother films. It is possible that adjacent azo-benzene molecules shift longitudinally relative to each other. We test this idea by calculating the energy difference between the dimers oriented parallel versus the case where one of the pair is longitudinally shifted (see Fig. 5). For an arbitrary and rather drastic longitudinal shift of 5 Å, this longitudinally shifted configuration is energetically favorable for all the azo-benzene derivatives except for the tightly packed CH_3CO case. The antiparallel orientation of CH_3CO prefers a denser packing than in the shifted dipole configuration. Fig. 8B shows the tendency for the total energy to decrease as one member of the completely parallel dimer is shifted longitudinally. The tendency to shift longitudinally implies that these azo-benzene derivatives will

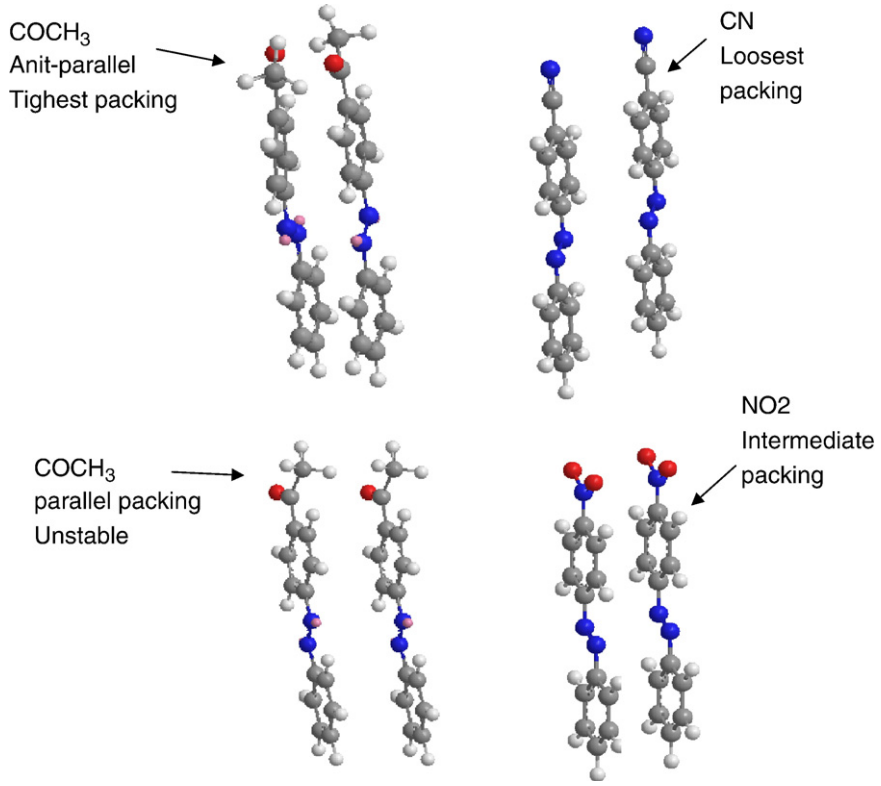

Fig. 7. Schematic representation of possible intermolecular orientations for CN-azo-$(CH_2)_{10}$–SO_3^-; and NO_2-azo $(CH_2)_{10}$–SO_3^-; and CH_3CO-azo-$(CH_2)_{10}$–SO_3^- dimers.

form unlevel L–B films. The simulation results reveal that the small dipoles reside on the antiparallel configured CH_3CO-azo-$(CH_2)_{10}$–SO_3 plays a critical role in promoting the packing density by lowering the dimerization energy and inhibits the CH_3CO-azo-$(CH_2)_{10}$–SO_3 molecules to shift away from each other, longitudinally. This is a very important yet an unexpected result which poses significant impact in design synthesis of molecular building blocks for creating functional structures via self-assembly method.

Predictions for the absorption maxima are presented in Table 2. All monomer units of azo-benzene derivatives have single strongly optically allowed singlet excited state responsible for the lowest frequency peak in experimental absorption spectra. Dimerization of molecular structures results in a splitting of this excitation into two excited states, where only the blue-shifted state is optically accessible (H-aggregation). The BHandHLYP [25] functional is then necessary to eliminate spurious intermolecular charge transfer states. However, this functional typically overestimates excited state energies and is generally not as accurate as the commonly used B3LYP one. For example, calculated excitation energies of monomers are blue shifted by 0.3–0.5 eV compared to experimental values. Nevertheless, we observe trends consistent with experimental data. Solvent stabilizes excitation energies by 0.1–0.2 eV and further improves agreement with experiment. The PCM model used for the solvent effects should be qualitatively if not quantitatively accurate.

Table 2 clearly shows that all optically active states of aggregates (films) are blue shifted compared to the molecules in solvent. For example, for the CN derivative, the experimental shift of the absorption peak in the film relative to the peak in solution is 0.05 eV. According to our calculations, a much larger shift of about 0.26 eV at 4 Å spacing could be expected in a completely smooth film. We have arrived at this estimate by taking double the shift from monomer to dimer (0.13 eV) according to Hückel theory. The solvent stabilizes the excitation energy by 0.15 eV. The discrepancy between the experiment and theory can be attributed to the torsional disorder of molecules in a solvent. Indeed, the potential energy surface of azo-benzenes with respect to rotation around N═N bond is very flat. The molecule being excited typically undergoes *trans–cis* photoisemerization in solution. Subsequently linear absorption spectra sample statistical ensemble where the flat structure considered in theory has the lowest excitation energy. Furthermore, the packing in the film is unknown. If we assume that adjacent CN monomers are shifted longitudinally relative to each other, we can easily account for the experimental results at the given intermolecular separation of 4 Å. Since the longitudinal shift reduces the dimerization of the excited states to a large extent, and at a large longitudinal shift, the energy of the optically active singlet state is hardly effected. A similar story unfolds for the NO_2 derivative. The experimental shift is 0.26 eV. The theoretical solvation shift is 0.22 eV to the red and the aggregation shift is on the order of 0.26 eV to the blue at parallel configuration and 4 Å separation. The latter reduces to 0.1 eV with an upward shift of nearest neighbors by 5 Å. These trends are in a good agreement with observed experimental shift and presumed packing model (Fig. 5). Finally, the $COCH_3$ experimental shift is 0.74 eV. At the intermolecular spacing of 4 Å and with a smooth film packing, we predict a shift of about 0.35 eV, which is only about half the experimental shift. As the intermolecular spacing is reduced we expect a drastic blue shift and that our prediction will become comparable to experiment at spacings shorter than 4 Å. However, the predictive power of the BHandHLYP functional breaks down at shorter intermolecular spacing due to the appearance of spurious charge transfer states, and extrapolation is necessary.

Table 2
Calculated and experimental values of excitation energies (in eV) of optically active excited states for unshifted and shifted azo-benzene derivatives

	Theory (monomer)		Experiment		Theory (dimers unshifted)			Theory (dimers shifted by 5 Å)		
X	Vacuo	Solvent	Solvent	Film	4 Å	6 Å	8 Å	4 Å	6 Å	8 Å
CN	3.90	3.75	3.39	3.44	4.03	3.98	3.95	3.92	3.93	3.92
NO_2	3.72	3.50	3.27	3.53	3.85	3.80	3.76	3.7[a]	3.75	3.74
$COCH_3$ p	3.88	3.73	3.39	4.13	4.01	3.96	3.92	3.89	3.91	3.91
$COCH_3$ ap	3.88	3.73	3.39	4.13	3.98	3.96	3.92	3.91	3.91	3.91

All calculations of dimer structures were done in vacuo. The notation p refers the configuration in which the acetyl groups are oriented parallel, and ap refers to the energetically favorable anti-parallel configuration.
[a] This result is inaccurate due to charge transfer problems.

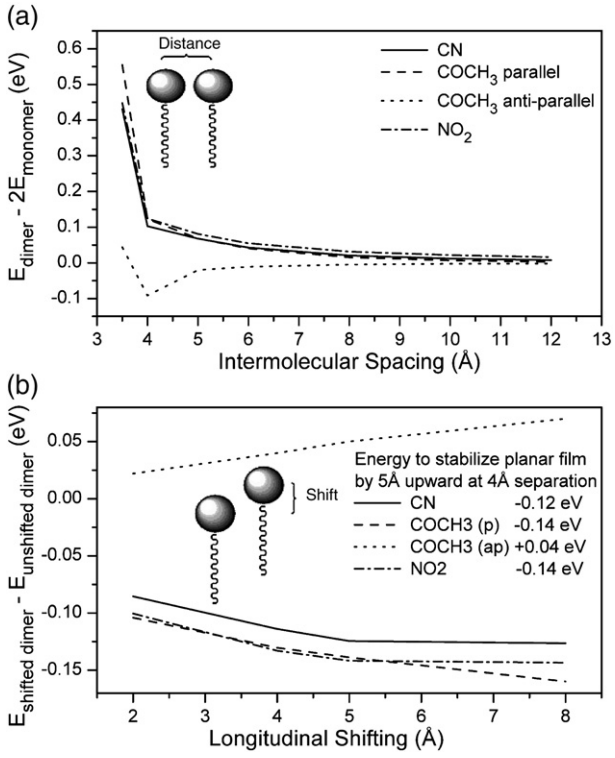

Fig. 8. (a) Plot of dimerization energy as a function of distance between two amphiphilic molecules. (b) Plot of dimerization energy as a function of the distance as one molecule drifts away in the longitudinal direction.

4. Conclusion

In this paper, we have demonstrated that the interplay between noncovalent forces such as dipole–dipole and π−π interactions

dominates the packing density, structures, and electronic properties of nanoassemblies prepared using the L–B method. In CH_3CO-azo-$(CH_2)_{10}$–SO_3^- dipole–dipole interactions can be reduced by specific packing pattern and overwhelmed by the strong π−π interaction between azo-benzene chromophores leading to prominent H-aggregation formation at the air–water interface. In other cases (CN-azo-$(CH_2)_{10}$–SO_3^- and NO_2-azo-$(CH_2)_{10}$–SO_3^-) strong dipole–dipole interaction leads to the formation of a staggered and more loosely packed monolayer at the air–water interface. Loosely packed L–B films show neither the H-aggregate formation nor electronic coupling between chromophores. Simulation results indicate that internal dipoles residing within acetyl groups registered in an antiparallel orientation significantly lower the total energy of a dimer system. The anti-parallel configuration also inhibits the CH_3CO-azo-$(CH_2)_{10}$–SO_3 molecules to shift away from each other, longitudinally. The simulation results further explain the fact that CH_3CO-azo-$(CH_2)_{10}$–SO_3 has a densely packed monolayer and displays a strong blue shift in absorption spectrum resulting from the formation of H-aggregates.

Our work demonstrates a way to control formation of nano-scaled structures through the control of noncovalent interactions. Tuning non-covalent interactions within such assemblies is important for controlling the internal morphology, which in turn will determine bulk properties such as conductivity and optical nonlinearity, as well as the mechanical properties of the assembly. Specifically, in this work we have shown how desirable non-covalent interactions may lead to highly ordered materials with large second-ordered susceptibilities. Finally, the understanding achieved through this work will allow us to predict and promote structural order both on the molecular level and the macro scale in the L–B films.

Acknowledgments

The work is supported by the Center for Nonlinear Studies (CNLS), the LDRD program of Los Alamos National Laboratory, and the Basic Energy Science, Office of Science (DOE).

References

[1] S.R. Marder, B. Kippelen, A.K.Y. Jen, N. Peyghambarian, Nature 388 (1997) 845.
[2] D.M. Burland, R.D. Miller, C.A. Walsh, Chem. Rev. 94 (1994) 31.
[3] M.H. Liu, K. Ushida, A. Kira, H. Nakahara, J. Phys. Chem., B Mater. Surf. Interfaces Biophys. 101 (1997) 1101.
[4] K. Owaku, M. Goto, Y. Ikariyama, M. Aizawa, Sens. Actuators, B, Chem. B14 (1993) 732.
[5] M.S. Johal, Y.W. Cao, X.D. Chai, L.B. Smilowitz, J.M. Robinson, T.J. Li, D. McBranch, D.Q. Li, Chem. Mater. 11 (1999) 1962.
[6] D.Q. Li, T.J. Marks, T.G. Zhang, G.K. Wong, Synth. Met. 43 (1991) 3157.
[7] J.M. Cole, Philos. Trans. - Royal Soc. Lond., Ser. A: Math. Phys. Eng. Sci. 361 (2003) 2751.
[8] D.F. Eaton, G.R. Meredith, J.S. Miller, Adv. Mater. 4 (1992) 45.
[9] L. Dalton, Polym. Photonics Appl. I 158 (2002) 1.
[10] A. Ulman, An Introduction to Ultrathin Organic Films: From Langmuir to Self-Assembly, Academic Press, Inc., San Diego, 1991.
[11] I.R. Peterson, J. Phys., D, Appl. Phys. 23 (1990) 379.
[12] J.A. Zasadzinski, R. Viswanathan, L. Madsen, J. Garnaes, D.K. Schwartz, Science 263 (1994) 1726.
[13] Y. Wang, X.J. Wang, Y. Guo, Z.C. Cui, Q. Lin, W.Z. Yu, L.Y. Liu, L. Xu, D.M. Zhang, B. Yang, Langmuir 20 (2004) 8952.
[14] D. Mobius, Langmuir–Blodgett Films, Plenum, New York, 1990.
[15] M.S. Johal, A.N. Parikh, Y. Lee, J.L. Casson, L. Foster, B.I. Swanson, D.W. McBranch, D.Q. Li, J.M. Robinson, Langmuir 15 (1999) 1275.
[16] C. Li, B. Zhao, Y.Q. Lu, Y.Q. Liang, J. Colloid Interface Sci. 235 (2001) 59.
[17] S. Dante, R. Advincula, C.W. Frank, P. Stroeve, Langmuir 15 (1999) 193.
[18] N.G. Caculitan, P.H. Scudder, A. Rodriguez, J.L. Casson, H.L. Wang, J.M. Robinson, M.S. Johal, Langmuir 20 (2004) 8735.
[19] H. Kuhn, C. Kuhn, Chromophore Coupling Effects, In J-Aggregates, World Scientific, Singapore, 1996.
[20] A. Ault, Techniques and Experiments for Organic Chemistry, 4th ed.Allyn & Bacon Inc., Boston, 1983.
[21] Y.C. Chao, T.S. Lee, S.Y. Chang, Dyes Pigm. 37 (1998) 255.
[22] J.V. Crivello, M. Deptolla, H. Ringsdorf, Liquid Cryst. 3 (1988) 235.
[23] R. Lantzsch, A. Marhold, K. Lehment, German (1977).
[24] M.E. Casida, Recent Advances in Density-Functional Methods, vol. 3, World Scientific, Singapore, 1995.
[25] A.D. Becke, J. Chem. Phys. 98 (1993) 5648.
[26] E. Runge, E.K.U. Gross, Phys. Rev. Lett. 52 (1984) 997.
[27] M.J. Frisch, Gaussian 98, Revision A.11. Gaussian, Inc., Pittsburgh, 1998.
[28] E. Cances, B. Mennucci, J. Tomasi, J. Chem. Phys. 107 (1997) 3032.
[29] M. Cossi, V. Barone, J. Chem. Phys. 115 (2001) 4708.
[30] C.P. Smith, Dielectric Behavior and Structure, McGraw-Hill, New York, 1955.